NASA TN D-1920

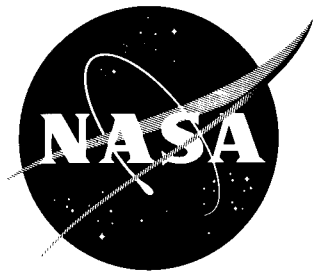

TECHNICAL NOTE

D-1920

ANALYSIS OF AXISYMMETRIC, ROTATING PRESSURIZED FILAMENTARY STRUCTURES

By

O. R. Burggraf and H. U. Schuerch

Prepared under Contract NASr-8 by
ASTRO RESEARCH CORPORATION
Santa Barbara, California
for
NATIONAL AERONAUTICS AND SPACE ADMINISTRATION
WASHINGTON

May 1963

TABLE OF CONTENTS

LIST OF ILLUSTRATIONS

NATIONAL AERONAUTICS AND SPACE ADMINISTRATION

TECHNICAL NOTE D-1920

ANALYSIS OF AXISYMMETRIC, ROTATING PRESSURIZED FILAMENTARY STRUCTURES

By

O. R. Burggraf and H. U. Schuerch

SUMMARY

An analytic treatment of the equilibrium configurations for thin-walled, axisymmetric, rotating, filamentary pressure vessels is presented. Solutions in the form of tabulated elliptical integral functions are developed for the pertinent geometrical characteristics of the structural shapes and for their associated filamentary geometries. A morphological review of the corresponding structures is presented, based upon a discussion of the mathematical properties of the solutions.

Experimental realization of the equilibrium configuration of a single filament subject to a centrifugal force field confirms the validity of analytic expressions.

Applications of formulas to problems of external loadings and of the static stability of filamentary, pressure stabilized structures demonstrate the utility of the analytical technique.

INTRODUCTION

The use of filamentary structures is of continually increasing interest for applications requiring ultimate structural performance, and is made possible by exploiting the remarkable physical properties of materials in the form of thin, continuous fibers. Theories for stresses and deformations in such structures are based upon two basically different approaches: analysis from the point of view of reinforced, anisotropic shell theory or, alternatively, from considerations of individual filaments.

With the first method, stresses in the matrix material are easily accommodated, thus allowing great generality. A fundamental treatment of this type of problem is given by Green & Adkins (Reference 1) in a chapter on reinforced materials. A similar treatment applied to orthotropic materials is given, for instance, by Harmon in Reference 2.

With the second method, the matrix material usually is assumed to be completely compliant, the tension in the filament being the dominant load carrying stress in the structure. The filament analysis, though more restricted, is simpler to apply and more readily yields usable information. Thus, the case of filament wound structures, subject to pure pressure loading, has been analyzed in detail. The resulting concept of monotropic membranes as structural elements, and their analytic treatment, has been presented by the authors in Reference 3. The special case of isotensoid structures, representing an optimum design configuration due to the uniformity of filament stress, has been discussed by Hoffman and Schuerch in References 4 and 5, and for the special case of filament wound pressure vessel end closures, by Zickel in Reference 6.

In many proposed applications of filamentary structures, centrifugal loading of the filaments is expected to be important. The basic equilibrium conditions for combined pressure and centrifugal loading were given in Reference 3; however, in further analysis of the filament geometry, only pressure loading was considered. The present report is concerned with analyzing the effects of centrifugal loading on filament wound pressurized structures.

In contrast to Reference 3, wherein numerical results were obtained by integrating the equilibrium equations on a digital computer, the present report gives the results in the form of analytic expressions involving tabulated functions. The results of Reference 3 may be obtained from these formulas as a special case. As a further distinction, the basic differential equations for monotropic membranes were developed in Reference 3 from differential geometrical considerations of lines on surfaces without initial restriction to surfaces of revolution. An alternate derivation of the equilibrium condition for the particularly interesting case of surfaces of revolution is given here for the sake of completeness.

LIST OF SYMBOLS

C	$= \sin\beta_o$
$E(\psi, k)$, $E(k)$	elliptic integrals of second kind
$F_{(\psi, k)}$, $F_{(k)}$	elliptic integrals of the first kind
H	see equation (17c)
J_n	integral defined by equation (20)
K	$= \dfrac{2\pi p_o r_o^2}{nT}$, pressure parameter
k	modulus of elliptic integral
ℓ	filament length
L	$= \ell / r_o$
m'	filament mass per unit length
n	number of windings
N	force on filament
p	pressure (p_o = pressure at $r = r_o$)
r	radius from axis of symmetry
r_o	equatorial radius
R	$= r / r_o$
T	tension in filament
T_o	tension at $r = r_o$
x	$= R^2$
x_2, x_3	see equations (17)

LIST OF SYMBOLS (Continued)

y	see equation (16)
z	distance along axis of symmetry
Z	$= z/r_o$
α	angle between tangent to meridian curve and z axis
β	helix angle
$\Lambda_o(\psi, k)$	Heuman Lambda Function, see equation (27)
$\Pi(\psi, \alpha^2, k)$, $\Pi(\alpha^2, k)$	elliptic integrals of third kind
φ	central angle
Ω	$m' r_o^2 \omega^2 / T_o$, centrifugal loading parameter
ω	angular velocity
ρ_f	density of fluid

I. BASIC DIFFERENTIAL EQUATIONS

A. Equilibrium Conditions

Consider a uniformly spaced array of n filaments placed on a surface of revolution as shown in Figure 1. If the spacing is small, the filaments will constitute a structure that can be described as a monotropic membrane (Reference 3). Assume this structure to be subject to loads generated by an internal positive pressure p, and by rotation with angular velocity ω around the z-axis. Assume further that a non-structural liner contains the internal pressure and distributes the pressure loads equally among the filaments without further contribution to the load carrying function of the structure.

Now consider an individual filament as a completely flexible but axially stiff structural element. To determine filament shape, apply 3 independent equilibrium conditions: (1) equilibrium of torques about the z-axis; (2) equilibrium of forces in the z direction; and (3) equilibrium of forces parallel to the filament. To apply these equilibrium conditions, the corresponding force components are needed. Referring to Figure 2 for notation, the components of the tension in the filament are simply

$$T_\varphi = T \sin\beta \tag{1a}$$

$$T_z = T \cos\beta \cos\alpha \tag{1b}$$

$$T_r = T \cos\beta \sin\alpha \quad . \tag{1c}$$

The pressure force affects only the equilibrium of forces in the z direction. The angular separation between adjacent filaments is $2\pi/n$, where n is the number of filaments crossing the plane $z=0$. Hence the distance separating the filaments at radius r is just $2\pi r/n$, and the z components of the pressure force on a filament per differential increment of radius is given by

$$dN_z = \frac{2\pi pr}{n}\, dr \quad . \tag{2}$$

The centrifugal force affects only the equilibrium condition along the axis of the filament, so that only the component parallel to the filament is needed. The centrifugal force for a length $d\ell$ of filament of linear density m' is

$$dN = m' r \omega^2 d\ell$$

where ω is the angular velocity of the filament about the z-axis. This

radial vector resolves parallel to the filament to give

$$dN_T = (m' r \omega^2 d\ell) \sin\alpha \cos\beta \quad .$$

Since the element of length $d\ell$ resolves along the radius vector according to

$$d\ell \sin\alpha \cos\beta = -dr \quad ,$$

the component of centrifugal force parallel to the filament is given by

$$dN_T = - m' r \omega^2 dr \quad . \tag{3}$$

With these expressions for the force components, the equilibrium conditions are now readily obtained. Since only the tension in the filament produces a torque about the z-axis, equilibrium in torque requires that rT_φ be constant along the filament, or

$$T r \sin\beta = T_o r_o \sin\beta_o \quad , \tag{4}$$

where the constant has been evaluated at $z=0$.* For equilibrium of forces in the z direction, only the filament tension and pressure force contribute. Hence, from equations (1b) and (2),

$$\frac{d}{dr} (T \cos\beta \cos\alpha) = \frac{2\pi p r}{n} \quad . \tag{5}$$

The final condition of equilibrium of forces parallel to the filament involves only filament tension and centrifugal force. From equation (3) there results

$$\frac{dT}{dr} = - m' r \omega^2 \quad . \tag{6}$$

B. Filament Orientation

Equation (6) may be integrated immediately to give

$$(T/T_o) = 1 + \frac{\Omega}{2} \left(1 - \frac{r^2}{r_o^2}\right) \quad , \tag{7}$$

where $\Omega = m' r_o^2 \omega^2 / T_o$.

---

* For isotensoids (T=const.) , equation (4) was obtained in Reference 3 from consideration of geodesic curves on a surface of revolution.

The constant of integration was evaluated at $z=0$. Introducing non-dimensional coordinates $R=r/r_o$ and $Z=z/r_o$, and the abbreviated notation $C=\sin\beta_o$, the azimuth angle β of the filament on its surface of revolution obtained from equation (4) becomes

$$\sin\beta = \frac{C}{R\left[1 + \frac{1}{2}\Omega(1 - R^2)\right]} \quad . \tag{8}$$

Finally, the integral of equation (5) is expressed as

$$T\cos\beta\cos\alpha = T_o\cos\beta_o + \frac{2\pi}{n}\int_r^{r_o} pr\,dr \tag{9}$$

(Note that $\alpha_o=0$ since $z=0$ is taken as the plane of symmetry). If the pressurizing fluid has density ρ_f , then the steady state pressure distribution is that for solid body rotation:

$$p = p_o + \frac{1}{2}\rho_f r^2\omega^2 \quad , \tag{10}$$

where p_o is the pressure on the axis of rotation. With this result, the integral in equation (9) may be evaluated. Thus, with $K=2\pi p_o r_o/n T_o$, equation (9) reduces to

$$\left(\frac{T}{T_o}\right)\cos\beta\cos\alpha = \cos\beta_o - \frac{1}{2}K(1 - R^2)\left[1 + \frac{1}{4}\frac{\rho_f \omega^2 r_o^2}{p_o}(1+R^2)\right] \quad . \tag{11}$$

Using equations (7) and (8), T and β may be eliminated:

$$\cos\alpha = \frac{\sqrt{1 - C^2} - \frac{1}{2}K(1-R^2)\left[1 + \frac{1}{4}\frac{\rho_f \omega^2 r_o^2}{p_o}(1+R^2)\right]}{\sqrt{\left[1 + \frac{1}{2}\Omega(1-R^2)\right]^2 - \frac{C^2}{R^2}}} \tag{12}$$

C. Filament Geometry

Although the orientation of the filament is determined completely by equations (8) and (12), its location in space is yet to be determined. The angles denoted in Figure 2 may be defined by the relations

$$\frac{dZ}{dR} = -\cot\alpha = \pm\frac{\cos\alpha}{\sqrt{1-\cos^2\alpha}}, \tag{13a}$$

$$R\frac{d\varphi}{dR} = -\tan\beta/\sin\alpha = \pm\frac{\sin\beta}{\sqrt{(1-\sin^2\beta)(1-\cos^2\alpha)}}. \tag{13b}$$

Thus, from equations (8), (12), and (13a) the meridian curve must satisfy

$$\frac{dZ}{dR} = \pm\frac{\sqrt{1-C^2} - \frac{1}{2}K(1-R^2)\left[1+\frac{1}{4}\frac{\rho_f\omega^2 r_o^2}{p_o}(1+R^2)\right]}{\sqrt{\left[1+\frac{1}{2}\Omega(1-R^2)\right]^2 - \frac{C^2}{R^2} - \left\{\sqrt{1-C^2} - \frac{1}{2}K(1-R^2)\left[1+\frac{1}{4}\frac{\rho_f\omega^2 r_o^2}{p_o}(1+R^2)\right]\right\}^2}}. \tag{14}$$

Similarly, from equations (8),)12), and (13b) the central angle φ must satisfy

$$\frac{d\varphi}{dR} = \pm\frac{C/R^2}{\sqrt{\left[1+\frac{1}{2}\Omega(1-R^2)\right]^2 - \frac{C^2}{R^2} - \left\{\sqrt{1-C^2} - \frac{1}{2}K(1-R^2)\left[1+\frac{\rho_f\omega^2 r_o^2}{p_o}\ 1+R^2)\right]\right\}^2}}. \tag{15}$$

The differential equations (14) and (15) completely determine the filament curves in space. The radicand in the denominators is a fifth-degree polynomial in R^2. Hence, the integrals for $Z_{(R^2)}$ and $\varphi_{(R^2)}$ are hyperelliptic integrals of class 2; evaluation of such integrals usually requires either numerical integration or complicated series expansion. However, closed form solutions in terms of tabulated functions may be obtained if the parameter $(\rho_f \omega^2 r_o^2/p_o)$ is set equal to zero, corresponding to a structure pressurized by a light fluid (or gas). The effect of centrifugal force then affects the filament geometry only through the parameter Ω. With this simplification, the radicand in the denominators becomes a cubic in R^2, and the integrals reduce to ordinary elliptic integrals. In the following, only the case $(\rho_f \omega^2 r_o^2/p_o = 0)$ will be considered.

II. INTEGRATION OF EQUATIONS

A. The Factored Cubic

The differential equations for the meridian curve and the central angle both contain as a denominator the quantity

$$y = \sqrt{(K^2-\Omega^2)x^3 - 4\left[\Omega\left(1+\frac{\Omega}{2}\right) + K\left(\sqrt{1-C^2}-\frac{K}{2}\right)\right]x^2 + 4\left[\left(1+\frac{\Omega}{2}\right)^2 - \left(\sqrt{1-C^2}-\frac{K}{2}\right)^2\right]x-4C^2} \quad , \tag{16}$$

where $x=R^2$, and where $(\rho_f \omega^2 r_o^2/p_o)$ has been set equal to zero. To facilitate integration of the equations, the factored form of the radicand is preferred. One root of the cubic radicand is $x_1=1$ corresponding to the previous choice of $z=0$ as plane of symmetry. Dividing out this root from the radicand leaves the quadratic

$$(K^2-\Omega^2)x^2 + 4\left[K\sqrt{1-C^2} + \Omega - \tfrac{1}{4}(K^2-\Omega^2)\right]x-4C^2 \quad .$$

The remaining two roots of the cubic are

$$x_2 = -\frac{2}{K^2-\Omega^2}\left\{H - \sqrt{H^2 + C^2(K^2-\Omega^2)}\right\} \quad , \tag{17a}$$

$$x_3 = -\frac{2}{K^2-\Omega^2}\left\{H + \sqrt{H^2 + C^2(K^2-\Omega^2)}\right\} \quad , \tag{17b}$$

where

$$H = K\sqrt{1-C^2} + \Omega - \tfrac{1}{4}(K^2-\Omega^2) \quad . \tag{17c}$$

Thus, in factored form

$$y = \sqrt{(K^2-\Omega^2)(1-x)(x-x_2)(x-x_3)} \quad . \tag{18}$$

The particular ordering of the roots indicated in equation (18) is not the only possible choice. Altogether, there are 24 permutations of the

inequality $x_3 < x_2 < x < 1$ providing positive values of the radicand (12 for $K > \Omega$ and 12 for $K < \Omega$). However, most of these permutations do not correspond to physically realizable values of Ω, K, and C for rotating, pressurized structures. A critical examination of equations (17) for the roots x_2 and x_3, outlined in Appendix A, reveals the following theorems which determine the acceptability of a given permutation of the roots:

Theorem A. For $K > \Omega$, $x_2 \geq 0$ and $x_3 \leq 0$ for all physically realizable values of K, Ω, and C.

Theorem B. For $K < \Omega$, $x_2 \geq 0$, $x_3 > x_2$ and also $x_3 > 1$ for all physically realizable values of K, Ω, and C.

In addition, the initial condition Z=0 at x=1 provides the condition: x and 1 cannot be separated by x_2 or x_3.

Application of these criteria shows that the only physically realizable orderings of the roots are the following:

$$\text{Case A:} \quad K > \Omega, \quad x_3 < x_2 < x < 1 \tag{19a}$$

$$\text{Case B:} \quad K > \Omega, \quad x_3 < 1 < x < x_2 \tag{19b}$$

$$\text{Case C:} \quad K < \Omega, \quad x_2 < x < 1 < x_3 \tag{19c}$$

$$\text{Case D:} \quad K < \Omega, \quad 1 < x < x_2 < x_3 \tag{19d}$$

A discussion of the physical significance of these distinct cases is deferred until the section on morphology of the structures. For the present, it is merely noted that the analytical form of the solution may be different for each of these four cases.

B. Meridian Curve

From the condition of axial symmetry, the filaments form a surface which may be considered to be generated by rotating a curve in a meridian plane ($\varphi = \text{const.}$) around the z axis. The slope of this meridian curve is given by equation (14), which reduces to ($\rho_f = 0$) :

$$\frac{dZ}{dx} = \pm \frac{\frac{1}{2}\left[\left(\sqrt{1 - C^2} - \frac{K}{2}\right) + \frac{K}{2}x\right]}{\sqrt{x\left[1 + \frac{1}{2}\Omega(1 - x)\right]^2 - C^2 - \left[\sqrt{1 - C^2} - \frac{K}{2}(1 - x)\right]^2}} \; .$$

With y defined by equation (16), introduce the notation

$$J_{n(x)} = \int_x^1 \frac{x^n\,dx}{y} \quad . \tag{20}$$

The meridian curve is given in terms of the J-integrals:

$$Z_{(x)} = \pm\left[\left(\frac{K}{2} - \sqrt{1 - C^2}\right) J_{o(x)} - \frac{K}{2} J_{1(x)}\right] \quad .$$

The J-integrals are evaluated in Appendix B for each of the four cases of equations (19). For Cases A and D, the meridian curves are given by

$$Z_{(x)} = \pm\frac{1}{\sqrt{(K^2-\Omega^2)(1-x_3)}}\left\{\left[K(1-x_3) - 2\sqrt{1-C^2}\right]F(\psi, k_1) - K(1-x_3)\,E(\psi_1, k_1)\right\} \quad , \tag{21}$$

where

$$\sin\psi_1 = \sqrt{\frac{1-x}{1-x_2}} \qquad \text{and} \qquad k_1 = \sqrt{\frac{1-x_2}{1-x_3}} \quad .$$

For the other two cases, the modulus k , becomes imaginary. Hence for Cases B and C, the alternate form of the integrals is used:

$$Z_{(x)} = \pm\frac{1}{\sqrt{(K^2-\Omega^2)(x_2-x_3)}}\left\{-\left[K(1-x_3) - 2\sqrt{1-C^2}\right]\left[F(k_2) - F(\psi_2, k_2)\right] + K(x_2-x_3)\left[E(k_2) - E(\psi_2, k_2)\right]\right\} \quad , \tag{22}$$

where

$$\sin\psi_2 = \sqrt{\frac{x_2-x}{x_2-1}} \qquad \text{and} \qquad k_2 = \sqrt{\frac{x_2-1}{x_2-x_3}} \quad .$$

An exceptional case remains for consideration: $K = \Omega$. By considering the limiting behavior of equations (17), the roots of the cubic are

found to go as

$$\lim_{K\to\Omega} x_2 = \frac{C^2}{\Omega(1+\sqrt{1-C^2})} , \tag{23a}$$

$$\lim_{K\to\Omega} x_3 = \pm\infty . \tag{23b}$$

Consider the form of solution given by equation (21); then

$$\lim_{K\to\Omega} \sqrt{(K^2-\Omega^2)(1-x_3)} = 2\sqrt{\Omega(1+\sqrt{1-C^2})},$$

and

$$\lim_{K\to\Omega} k_1 = 0 .$$

With the series expansions of the elliptic integrals

$$F(\psi,k) = \int_0^{\psi} \frac{d\psi}{\sqrt{1-k^2\sin^{-2}\psi}} = \psi + \frac{1}{4}k^2(\psi - \sin\psi\cos\psi) + - - - ,$$

$$E(\psi,k) = \int_0^{\psi} \sqrt{1-k^2\sin^2\psi}\, d\psi = \psi - \frac{1}{4}k^2(\psi - \sin\psi\cos\psi) + - - - ,$$

and with the above limiting values, the solution for $K=\Omega$ is found to be

$$Z = \pm\frac{1}{\sqrt{\Omega(1+\sqrt{1-C^2})}}\left\{\left[\frac{\Omega}{4}(1-x_2) - \sqrt{1-C^2}\right]\arcsin\sqrt{\frac{1-x}{1-x_2}} - \frac{\Omega}{4}\sqrt{(1-x)(x-x_2)}\right\} , \tag{24}$$

where x_2 is given by equations (23) above. For C=0 (meridian wrapped filaments) equation (24) reduces to

$$Z = \left\{\frac{1}{\sqrt{2\Omega}}\left(1-\frac{1}{4}\Omega\right)\arcsin\sqrt{1-x} + \frac{1}{8}\sqrt{2\Omega}\sqrt{x(1-x)}\right\} . \tag{25}$$

Equation (24) has been verified as the integral of equation (14) for $K=\Omega$ (with $\rho_f = 0$) by direct differentiation.

C. Central Angle

If the parameter C is not zero, the filament will advance around the z-axis as it is wound. The central angle φ (see Figure 2) is determined by integrating equation (15). In terms of the variable $x = R^2$, and for $\rho_f = 0$, this equation reduces to

$$\frac{d\varphi}{dx} = \pm \frac{C/2}{x\sqrt{x\left[1 + \frac{1}{2}\Omega(1 - x)\right]^2 - C^2 - x\left[\sqrt{1 - C^2} - \frac{1}{2}K(1 - x)\right]^2}} .$$

In terms of the J-integrals defined by equation (20), the central angle is given by

$$\varphi = \pm C \int_x^1 \frac{dx}{xy} = \pm C\, J_{-1}(x) . \tag{26}$$

As shown in Appendix B, the integral J_{-1} involves the incomplete elliptic integral of the third kind, which in turn involves Theta functions. These functions are tabulated in Reference 9, or alternatively can be evaluated by means of an infinite series. The complete integral may be evaluated in terms of Heuman's Lambda Function, Λ_o as in Appendix B, which is tabulated in Reference 7, for example. Λ_o is given in terms of the elliptic integrals of first and second kinds by

$$\frac{\pi}{2}\Lambda_o(\psi, k) = \left[E(k) - F(k)\right]F(\psi, k') + F(k)\, E(\psi, k'), \quad k' = \sqrt{1 - k^2} . \tag{27}$$

Thus for Case A (equation 19a), using equations (B-6) and (B-13), we obtain

$$\varphi_{(x_2)} = \pm \frac{\pi C}{\sqrt{-x_2 x_3 (K^2 - \Omega^2)}} \Lambda_o(\xi_1, k_1) , \tag{28a}$$

where

$$\sin\xi_1 = \sqrt{\frac{-x_3}{x_2 - x_3}} , \quad k_1 = \sqrt{\frac{1 - x_2}{1 - x_3}} .$$

For Case B, using equations (B-11) and (B-13)

$$\varphi_{(x_2)} = \mp \frac{\pi C}{\sqrt{-x_2 x_3 (K^2 - \Omega^2)}} \Lambda_o(\xi_2, k_2) , \tag{28b}$$

where

$$\sin\xi_2 = \sqrt{\frac{-x_3}{1 - x_3}} \quad , \quad k_2 = \sqrt{\frac{x_2 - 1}{x_2 - x_3}} \quad .$$

For Case C, using equations (B-11) and (B-14)

$$\varphi_{(x_2)} = \mp \frac{C}{\sqrt{\Omega^2 - K^2}} \left\{ \frac{2F(k_2)}{x_3\sqrt{x_3 - x_2}} + \frac{\pi}{\sqrt{x_2 x_3}} \Lambda_o(\eta_2, k_2) \right\} \quad , \qquad (28c)$$

where

$$\sin\eta_2 = \sqrt{\frac{x_3 - x_2}{x_3}} \quad , \quad k_2 = \sqrt{\frac{1 - x_2}{x_3 - x_2}} \quad .$$

For Case D, using equations (B-6) and (B-14)

$$\varphi_{(x_2)} = \pm \frac{C}{\sqrt{\Omega^2 - K^2}} \left\{ \frac{2F(k_1)}{x_3\sqrt{x_3 - 1}} + \frac{\pi}{\sqrt{x_2 x_3}} \Lambda_o(\eta_1, k_1) \right\} \quad , \qquad (28d)$$

where

$$\sin\eta_1 = \sqrt{\frac{x_3 - 1}{x_3}} \quad , \quad k_1 = \sqrt{\frac{x_2 - 1}{x_3 - 1}} \quad .$$

For the exceptional case $K = \Omega$, the incomplete integral may be evaluated in simple terms. Consider the central angle for Case A. Since $k_1 \to 0$ in the limit as $K \to \Omega$, we find (refer to Appendix B)

$$\Pi(\psi_1, \alpha_1^2, 0) = \int_0^{\psi_1} \frac{d\psi}{1 - \alpha_1^2 \sin^2\psi} = \frac{1}{\sqrt{1 - \alpha_1^2}} \arctan\left[\sqrt{1 - \alpha_1^2}\tan\psi_1\right] \quad .$$

Substituting into equation (26), by use of equation (B-6) and the limiting formulas given in equations (23) and following, the central angle is obtained as

$$\tan\varphi = C\sqrt{\frac{1 - x}{\left[\Omega(1 + \sqrt{1 - C^2})\, x - C^2\right]}} \quad . \qquad (29)$$

This formula evidently applies for all four cases of equations (19), in the limit $K = \Omega$. By letting $x \to x_2$ in equation (29), we observe that $\varphi \to \pi/2$; that is, in passing from outer radius to inner radius, the filament is wound a quarter turn about the z axis for the case $K = \Omega$, for any $C \neq 0$.

D. Filament Length

The space curve generated by a filament is completely determined by $Z_{(R)}$ and $\varphi_{(R)}$. However, for many purposes the filament length is needed also. For example, to determine how a given filament-wound structure will deform under various combinations of pressure and centrifugal loading, the filament length and advance angle (central angle φ per turn) must be held invariant. An expression for filament length is easily derived.

From Figure 2, the differential element of length dL (normalized with respect to equatorial radius r_o) is given by

$$dL \cos\beta \cos\alpha = dZ \quad .$$

Then, from equations (8), (12), and (14), with $\rho_f = 0$,

$$\frac{dL}{dx} = \pm \frac{(1 + \frac{1}{2}\Omega) - \frac{1}{2}\Omega x}{y} \quad , \tag{30}$$

where y is given by equation (16). In terms of J-integrals

$$L = \pm \left[(1 + \tfrac{1}{2}\Omega) J_o - \tfrac{1}{2}\Omega J_1 \right] \quad . \tag{31}$$

Hence, for Cases A and D, equations (19), substituting for J_o and J_1 from Appendix B, the filament length is given by (32)

$$L = \pm \frac{1}{\sqrt{(K^2-\Omega^2)(1-x_3)}} \left\{ 2F(\psi_1, k_1) + \Omega(1-x_3)\left[F(\psi_1, k_1) - E(\psi_1, k_1) \right] \right\} \quad ,$$

where

$$\sin\psi_1 = \sqrt{\frac{1-x}{1-x_2}} \quad \text{and} \quad k_1 = \sqrt{\frac{1-x_2}{1-x_3}} \quad .$$

For Cases B and C, equations (19), the alternate form of J_o and J_1 given in Appendix B should be used, resulting in the formula (33)

$$L = \pm \frac{1}{\sqrt{(K^2-\Omega^2)(x_2-x_3)}} \left\{ \left[2+\Omega(1-x_3) \right] F(\psi_2, k_2) - \Omega(x_2-x_3)\, E(\psi_2, k_2) \right\} \quad ,$$

where

$$\sin\psi_2 = \sqrt{\frac{x_2-x}{x_2-1}} \quad \text{and} \quad k_2 = \sqrt{\frac{x_2-1}{x_2-x_3}} \quad .$$

The exceptional case $K = \Omega$ may be evaluated as a limiting process as previously demonstrated for equation (24) for the meridian curve and

equation (29) for the central angle. Thus in the limit as $K \to \Omega$, equation (32) takes the form

(34)

$$L = \frac{\pm 1}{\sqrt{\Omega(1+\sqrt{1-C^2})}} \left\{ \left[1+\frac{1}{4}\Omega(1-x_2) \right] \arcsin\sqrt{\frac{1-x}{1-x_2}} - \frac{1}{4}\Omega \sqrt{(1-x)(x-x_2)} \right\} ,$$

with x_2 given by equation (23).

III. DISCUSSION OF RESULTS

A. Classification of Meridional Shapes

A morphology of axisymmetric filament-wound structures can be developed by discussing the range of possible solutions for the meridian given in equations (21), (22), or (24). These equations show the meridional shape to depend on the three characteristic parameters, K, Ω, and C, which define the pressure load intensity, the centrifugal load intensity, and the angularity of the winding pattern respectively.

For the purpose of this discussion, it will be assumed that both K and Ω are positive (or zero), corresponding to positive internal pressure and to tensile rather than compressive forces acting in the filaments. The range of possible solutions, then, can be grouped into two classes of periodic functions according to their topological characteristics. The two classes can be described as "undulating" (Figure 3) and "looped," (Figure 4). The corresponding surfaces of revolution are of the nature of corrugated tubes and toroids respectively.

The two classes of meridional curves are separated by the transitional case of a cusped function (Figure 3e) and bounded by a degenerate periodic function which, in the case of the undulating species, assumes the shape of a hyperbola, (Figure 3a); in the case of the looped species, it assumes the shape of a single loop with asymptotic branches (Figure 4d).

Each class can be further grouped into two types. The undulating class may be "waisted" such that the reference radius r_o is a minimum and $R \geq 1$ (Figure 3b); or it may be "bellied" such that the reference radius is a maximum and $R \leq 1$ (Figure 3c). The transitional case for the two types is the straight line $R \equiv 1$, corresponding to the meridian of a right circular cylinder (Figure 3c). The looped class may be "progressive," (Figure 4a) such that subsequent ordinates of $R = 1$ follow at values of increasingly larger positive Z if the curve is started at the coordinate $R = 1$, $Z = 0$, and followed in a direction of initially increasing Z; or it may be "regressive" (Figure 4c) in the sense that subsequent ordinates of $R = 1$ follow at increasingly negative Z. The transitional case for these two types is the closed loop forming the meridian of a smooth toroid (Figure 4b).

A summary of the possible meridional forms is given in Table I below.

TABLE I

Class:	Undulating			Looped		
Type:		Waisted	Bellied	Progressive	Regressive	
Limiting & Transition Case:	Hyperboloid	Cylinder	Cusp	Toroid		Asymptotic Loop

A discussion of the transition cases is useful in defining the domains of existence of the various types in the $K - C - \Omega$ space. By studying these singular types, the ranges of K, Ω, and C corresponding to the various classes of meridian curves may be established:

1. Hyperboloid

The hyperboloid corresponds to tension infinitely greater than the pressure or centrifugal force. Hence the hyperboloid requires $K = 0$, $\Omega = 0$.

2. Cylinder

The cylinder is defined by constant radius which requires $x_2 = 1$. This condition is analyzed in Appendix A, resulting in the condition

$$\Omega = C^2 - K\sqrt{1 - C^2} \quad . \tag{35}$$

Evidently for cylinders, Ω cannot exceed unity for non-negative K.

3. Cusp

The cusp divides the corrugated tubes from the progressive loops, and requires the point of zero slope $(x = x_0)$ to coincide with the point of infinite slope $(x = x_2)$. This condition is analyzed in Appendix C, resulting in the condition

$$\Omega = \frac{K}{\sqrt{1-C^2}} \left\{ \frac{C^2}{1 - \frac{2}{K}\sqrt{1-C^2}} - 1 \right\} \quad . \tag{36}$$

Cusps occur for all values of Ω; in the limit $\Omega \to \infty$ equation (36) reduces to

$$K = 2\sqrt{1-C^2} \quad .$$

The limit $\Omega \to \infty$ may be viewed as the limit $T_o \to 0$ and $p_o \to 0$ such that K remains constant. Then the radius of curvature is zero at $x = 1$ and the filament lies along the radius.

4. Toroid

The closed loop divides the progressive loops from the regressive loops and is defined by the condition $Z_{(x_2)} = 0$, where Z is given by equations (21) and (22). These equations are transcendental and an iterative

technique must be used to determine closed loop conditions. * However, certain results may be obtained directly. For example, note that for $C = 1$, $K = 0$ is a solution of $Z_{(x_2)} = 0$ for any Ω. On the other hand, for large K, series expansion of the terms in equation (21) results in the condition

$$C \to \sqrt{\frac{2\Omega + 1}{3}} \tag{37}$$

in the limit $K \to \infty$. These two points will be useful in interpreting the behavior of the closed loop conditions for various values of Ω.

These classifications are summarized graphically in Figure 5, in which the domains of each type curve are indicated on a plot of K vs C with Ω as the parameter. The curves for $\Omega = 0$ are identical to those of Reference 3. The effects discussed above are evident in the graph. Thus, cylinders are possible for $0 \leq \Omega \leq 1$ while cusps are possible for all values of $\Omega \geq 0$.

The character of the closed loop boundary is drastically different for $\Omega \leq 1$ than for $\Omega > 1$. For $\Omega \leq 1$, the closed loop condition requires $K \to \infty$ for some $C \leq 1$, in accordance with equation (37). For $\Omega > 1$, however, this asymptote no longer exists $(C > 1)$ and the condition $K = 0$ at $C = 1$ for all Ω now dominates the behavior of the closed loop boundary for C near unity. In Figure 6, the closed loop boundaries are shown for $\Omega = 1$, 1.1, 1.2, and 1.5, clearly demonstrating this behavior.

B. Sample Results

Meridian curves are plotted in Figures 7 and 8 for the following cases:

(1) $C = 0$, $K = \Omega = 4$

(2) $C = 0$, $K = 0$, $\Omega = 4$

(3) $C = 0.5$, $K = \Omega = 4$

(4) $C = 0.5$, $K = 0$, $\Omega = 4$

The value $\Omega = 4$ was chosen for convenience. In particular, the value $Z_{(0)} = 0$ results for Case (1). Figure 7 shows the effect of pressure on a centrifugal

---

* For $\Omega = 0$, it is possible to express all parameters in terms of the modulus of the elliptic integrals as the only unknown, greatly reducing the labor in calculating closed loop conditions.

loaded filamentary structure. In general a more convex shape results, as expected. Note that the two curves of Figure 7 are not the same structure since the filament length is different for the two cases. By scaling to the same filament length, the equatorial radius would be different for the pressurized vs unpressurized structure. Figure 8 shows the same effect when the filament is not meridian wrapped. The general shape of the meridian curve is the same as for $C = 0$ except in the vicinity of the axis. A central hole must exist for any helix-wound filamentary structure since the filaments cannot intersect the axis of rotation (except for $C = 0$). Note that in Figure 8 the curve for $K = 0$ is a corrugated tube and the curve for $K = 4$ is a regressive loop, as indicated by the domains in Figure 5.

IV. EXPERIMENT

For the purpose of realizing the analytically predicted geometry of a rotating filament, the simple case of $K = 0$, $\Omega = 4$ and $C = .5$ was chosen. This choice was made, since results from experimentation with non-rotating pressure vessels ($K > 0$, $\Omega = 0$) has been reported by the authors previously (Reference 3).

Non-dimensional ordinate Z , arc length L , and central angle φ were computed for the abscissa $R = .4$ from equations (22), (33), and (28c) respectively, yielding:

$$Z = .46$$

$$L = .87$$

$$\varphi = 29^{\circ}$$

To generate the corresponding geometry, a metal chain of appropriate length was supported on two disks with the attachment points rotated and spaced relative to each other by the indicated central angle and distance. The disks, in turn, were supported by a quill mounted into the spindle of a modified lathe, equipped with a variable speed drive. The test equipment with rotating chain is shown in a time exposure photograph by Figure 9. A flash exposure photograph of the same setup, revealing the instantaneous geometry assumed by the chain, is shown in Figure 10.

The geometry of the rotating chain was recorded by photography, using both flash and time exposures to obtain end view, side view, and envelope contour of the rotating chain. Figures 11a-c show typical records obtained by this means. The reference grid shown on Figures 11a and 11c was obtained by double exposure. For this purpose, the quill assembly was removed from the fixture after the first exposure of the rotating chain on a tripod-mounted Polaroid camera. An inked reference grid was then placed into the appropriate normal or axial center plane of the body of revolution generated by the revolving chain to minimize parallax errors. The camera shutter was then tripped for the second exposure of the film.

A theoretical computation was made for the end view, side view, and envelope contour (meridional shape) for the selected parameter triplet. The results of this computation, together with experimental data points obtained from the photographic records in Figures 11a-c are shown in Figure 12. In the process of data reduction, the side view of Figure 11b was corrected by a geometrical rotation to compensate for a slight delay in the timing of the exposure flash. All other data were obtained by directly plotting chain coordinates evaluated from the photographs onto the graph in Figure 12. The experimentally obtained data were found to agree with the theoretically predicted geometrical shapes within reading accuracy of the photographic records.

V. APPLICATION

Applications for the analytical techniques presented in this report fall into two broad categories: the design synthesis of optimized filamentary structures, in which the structural properties of the filaments are utilized to the fullest possible extent; and the study of specific problems arising in the structural analysis of filamentary structures. The latter application is of particular interest in the case of large elastic deformations observed in pressure stabilized structures subject to external loads, and in the study of the static stability of such structures.

In the treatment of these problems of analysis, the assumption may be made that the filaments remain inextensional and completely compliant in bending, and that the matrix or liner material remains stress-free during the deformation. With these assumptions, a point of departure for analysis is found in the intrinsic properties of the filamentary structure, i. e., in the properties which will not change during the deformation process. Such intrinsic properties are either topological or metric in nature.

Retention of intrinsic topological properties as they apply to the overall structural configuration will form, in general, the end points or constraints of possible deformation (i. e., a toroid will reamin a toroid throughout the deformation). Intrinsic topological properties, as they apply to the filamentary geometry, are of somewhat more subtle character and involve, for instance, the number of turns of the filament around the structure, and the periodicity of the turns per revolution. This characteristic is particularly evident in the case of the smooth toroid, where the number of filament turns around the toroid necessary to complete a full revolution of the central angle φ in the winding pattern constitutes an intrinsic property of the filamentary structure.

Intrinsic metric properties are, according to the assumptions of inextensional fibers stated above, the lengths of the filaments. Additional intrinsic metric properties may be stated for specific problems, such as a condition that cross-over points of differently oriented filament systems may not slide with respect to each other (trellis-condition).

The problem of structural analysis of a given filamentary structure, subject, for instance, to an external load thus reduces to finding related structural configurations with appropriately identical intrinsic properties, and with the required discontinuities at the locations of load application.

For the purpose of illustration, two examples for this type of analysis are summarized here. The first example considers a structural element consisting of a non-rotating ($\Omega = 0$) bottle-shaped pressure vessel with meridional windings ($C = 0$) anchored at two circumferential rings ($C = 1$) as shown in the inset of Figure 13. This element can be considered as either

representing the structural portion of a spheroidal rocket motor case, or can be considered as an element of a "corrugated" structural column.

Consider now this structure subject to an axial load P. The deformed configuration will retain the length of the filament between the rings and the circumferential length of the rings. Since the nature of the deformation is such that axisymmetry is retained, the possible shapes of deformation can be established by holding the filament length of the meridian and the radius of the rings invariant, for a range of selected K-values, which in this case are conveniently normalized for the invariant ring radius. Results of this procedure, in terms of normalized load-deformation characteristics and for an arbitrarily assumed constant internal pressure are shown in Figure 13, indicating the expected non-linear elastic behavior of the structure similar to that studied in detail in Reference 8.

The second example considers a range of non-rotating pressurized toroids formed by two branches of a meridional winding pattern joining an outer and inner equatorial ring, as shown in the inset of Figure 14. The toroids are designed for parameter values of $K = 5$, $C = 0$, $\Omega = 0$ in a condition without externally applied loads. A range of designs is generated by varying the intercept location of the two branches, or, in other terms, the radii r_1 and r_2 of the outer and inner equatorial rings. These radii are related to the ring cross sections (or number of filament turns n_1 and n_2) by the condition that the stress level in the fibers forming the equatorial bands be equal to the stress level in the fibers forming the meridional winding pattern (isotensoid condition).

An axisymmetrically distributed and axial loading P is considered, acting at the outer ring and reacted by an equal and opposite load applied at the inner ring. The question considered here is that of initial spring rate (i. e., the stiffness for small deformations from the unloaded equilibrium configuration) as it is affected by the particular choice of the ring radii and related number of turns in the rings. The results of this investigation, based upon intrinsically invariant filament length and assumption of invariant internal pressure, are shown in Figure 14. It will be observed that there exists a critical parameter configuration at which the spring rate vanishes, indicative of a state of marginal static stability of the structure. For negative spring rates, a statically unstable structure can be identified, exhibiting a "geometrical" instability in the sense that only geometrical and no material properties enter into the mechanism causing instability.

VI. CONCLUDING REMARKS

The filamentary structures considered in this report represent idealizations of actual structures in several respects; the importance of each will need to be assessed in specific applications in view of the individual case. The idealizations selected were such that relatively straightforward analytical formulation for the pertinent geometrical characteristics of the filamentary structures considered could be developed. These prove useful to gain insight into the general nature of the problems in design and operation of such structures.

In addition, the basic differential equations presented lend themselves to considerable generalization including the case of non-uniform internal pressure (of practical importance for rocket motors subject to distributed inertia loads and for the design of inserts and endclosure attachments). These problems can be readily solved by digital integration such as presented previously (Reference 3). The value of the analytical formulations in this case is that of allowing a check for the computor programs, by testing them on an idealized case for which the result can be readily verified analytically, as well as by providing means of initializing the digital programs.

Idealizations that may be serious limitations in specific applications rest in the basic concept of monotropic membrane arrays as representative for the structure. Where matrix materials of significant stiffness are used, the assumption that matrix materials will not contribute to the primary stress system must be questioned. Also inherent in the concept of monotropic membranes is the assumption of negligible wall thickness. For the case of thick-walled pressure vessels, specifically in areas of polar buildup due to cross-over of the winding pattern, a refined method somewhat reminiscent of a "stress concentration" analysis might be developed.

Finally, the case of deviations from axisymmetry remains to be studied from two points of view: the structure may originally be built with operationally required deviations from axisymmetry (as for instance, in the case of multiple nozzle and retro-ports in filament-wound solid propellant rocket motors); or non-axisymmetric loading on originally axisymmetric structures may cause deviations in the deformed state. A general approach to such problems, using the technique of differential geometry, has been outlined, but not implemented, in Reference 3. The mathematical difficulties, at first sight, appear formidable. Digital techniques, while cumbersome, may be developed to effectively solve critical problems in this area in the future.

Astro Research Corporation
Santa Barbara, California
September 30, 1962

APPENDIX A

PROPERTIES OF ROOTS x_2 AND x_3

The roots x_2 and x_3 are defined by equations (17) and repeated here for convenience:

$$x_2 = -\frac{2}{K^2 - \Omega^2}\left\{H - \sqrt{H^2 + C^2\,(K^2 - \Omega^2)}\right\},$$

$$x_3 = -\frac{2}{K^2 - \Omega^2}\left\{H + \sqrt{H^2 + C^2\,(K^2 - \Omega^2)}\right\},$$

where

$$H = K\sqrt{1 - C^2} + \Omega - \frac{1}{4}\,(K^2 - \Omega^2)\,.$$

In the following analysis, the parameters K and Ω will be assumed to be real, non-negative numbers, as required by their definitions as pressure and centrifugal loading parmeters with positive internal pressure, positive mass, and tensile filament forces. Also, the parameter C is limited to the range $0 \le C \le 1$ according to its definition: $C = \sin \beta_o$.

Consider first the case $K > \Omega$. Then H may be either positive or negative. For $H \le 0$, we must have $x_2 \ge 0$ (equality for $H = 0$, $C = 0$; hence also $K - \Omega = 4$).

Also $\sqrt{H^2 + C^2\,(K^2 - \Omega^2)} \ge |H|$, which requires $x_3 \le 0$ (equality for $C = 0$ only). Similarly for $H \ge 0$, we must have $x_3 \le 0$ (equality for $H = 0$, $C = 0$; hence also $K - \Omega = 4$), and also

$$\sqrt{H^2 + C^2\,(K^2 - \Omega^2)} \ge H\,,$$

which requires $x_2 \ge 0$ (equality for $C = 0$ only). Hence we have:

Theorem A. For $K > \Omega$, $x_2 \ge 0$ and $x_3 \le 0$ for all non-negative values of K and Ω.

Now consider the case $K < \Omega$. For this case H must be positive ($H > 0$). Hence $x_3 > 0$, and since

$$\sqrt{H^2 + C^2 (K^2 - \Omega^2)} \leq H \quad ,$$

we must have $x_2 \geq 0$ (equality for $C = 0$ only). Moreover $x_3 > x_2$.

It remains only to show that $x_3 > 1$ for all $K < \Omega$. For $C = 0$, we can write

$$H = (K + \Omega) \left[1 + \frac{1}{4} (\Omega - K) \right]$$

and

$$x_3 = \frac{4H}{\Omega^2 - K^2} = 1 + \frac{4}{\Omega - K} > 1 \quad ,$$

which holds for all K , Ω $(K < \Omega)$ for $C = 0$. Now hold K and Ω fixed and vary $C > 0$. If $x_3 < 1$ for some C (say C^1), then $x_3 = 1$ for some $C < C^1$.

Thus, it is sufficient to prove that $x_3 \neq 1$ for any C , K and Ω . Assume $x_3 = 1$; this requires

$$\left[\frac{\Omega^2 - K^2}{2} - H \right] = \sqrt{H^2 + C^2 (K^2 - \Omega^2)} \quad ,$$

or by squaring

$$\frac{\Omega^2 - K^2}{2} - (\Omega^2 - K^2) H = C^2 (K^2 - \Omega^2)$$

(Note that this squaring operation has removed the distinction between x_2 and x_3). Since $K \neq \Omega$

$$\frac{1}{4} (\Omega^2 - K^2) - H = C^2 \quad .$$

Substituting for H yields

$$\Omega = C^2 - K\sqrt{1 - C^2} \quad .$$

To determine whether this result corresponds to x_2 or x_3 , substitute it back into their definitions. We obtain

$$x_2 = 1$$

$$x_3 = \frac{4}{1 - \left(\sqrt{1 - C^2} + K\right)^2}$$

The latter equation permits no values of x_3 in the range $0 < x < 4$, which completes the proof. Thus we have:

Theorem B. For $K < \Omega$, $x_2 \geq 0$, $x_3 > x_2$, and also $x_3 > 1$ for all non-negative values of K and Ω.

APPENDIX B

EVALUATION OF J-INTEGRALS

Let the symbol $J_{n(x)}$ designate the integral

$$J_{n(x)} = \int_x^1 \frac{x^n}{y}\, dx \quad , \tag{B-1}$$

where

$$y = \sqrt{(K^2-\Omega^2)(1-x)(x-x_2)(x-x_3)} \quad . \tag{B-2}$$

The cases to be considered are $n=0$, 1 , and -1 .

Consider the variable

$$\sin\psi_1 = \sqrt{\frac{1-x}{1-x_2}} \quad . \tag{B-3}$$

In terms of ψ_1 , we find

$$y = \sqrt{(K^2-\Omega^2)(1-x_3)}(1-x_2)\sin\psi_1\cos\psi_1\sqrt{1-\left(\frac{1-x_2}{1-x_3}\right)\sin^2\psi_1} \quad .$$

Then denoting

$$k_1 = \sqrt{\frac{1-x_2}{1-x_3}} \quad ,$$

we find

$$J_o = \frac{2}{\sqrt{(K^2-\Omega^2)(1-x_3)}} \int_o^{\psi_1} \frac{d\psi}{\sqrt{1-k_1^2\sin^2\psi}} \quad ,$$

or

$$J_o = \frac{2}{\sqrt{(K^2-\Omega^2)(1-x_3)}}\, F(\psi_1, k_1) \quad , \tag{B-4}$$

where $F(\psi, k)$ is the incomplete elliptic integral of first kind (Reference 7).

Similarly

$$J_1 = \frac{2}{\sqrt{(K^2-\Omega^2)(1-x_3)}} \int_0^{\psi_1} \frac{1-(1-x_2)\sin^2\psi}{\sqrt{1-k_1^2\sin^2\psi}}\, d\psi$$

$$= \frac{2}{\sqrt{(K^2-\Omega^2)(1-x_3)}} \int_0^{\psi_1} \frac{x_3+(1-x_3)[1-k_1^2\sin^2\psi]}{\sqrt{1-k_1^2\sin^2\psi}}\, d\psi \quad ,$$

or

$$J_1 = \frac{2}{\sqrt{(K^2-\Omega^2)(1-x_3)}} \left[x_3 F(\psi_1, k_1) + (1-x_3) E(\psi_1, k_1)\right] \quad , \qquad \text{(B-5)}$$

where $E(\psi, k)$ is the incomplete elliptic integral of second kind. Finally

$$J_{-1} = \frac{2}{\sqrt{(K^2-\Omega^2)(1-x_3)}} \int_0^{\psi_1} \frac{d\psi}{\left[1-(1-x_2)\sin^2\psi\right]\sqrt{1-k_1^2\sin^2\psi}} \quad ,$$

or

$$J_{-1} = \frac{2}{\sqrt{(K^2-\Omega^2)(1-x_3)}} \Pi\ (\psi_1, \alpha_1^2, k_1) \quad , \qquad \text{(B-6)}$$

where $\Pi(\psi_1, \alpha_1^2, k)$ is the incomplete elliptic integral of third kind, and

$$\alpha_1^2 = 1 - x_2 \quad . \qquad \text{(B-7)}$$

These equations are in a form suitable for the two cases $K > \Omega$, $x_3 < x_2 < x < 1$, and $K < \Omega$, $1 < x < x_2 < x_3$. For the remaining two cases, an alternate form of these integrals is required.

Consider now the variable

$$\sin\psi_2 = \sqrt{\frac{x_2 - x}{x_2 - 1}} \quad . \qquad \text{(B-8)}$$

Then in terms of ψ_2 , y becomes

$$y = \sqrt{(K^2-\Omega^2)(x_2-x_3)(x_2-1)}\,\sin\psi_2\cos\psi_2\sqrt{1-\frac{x_2-1}{x_2-x_3}\sin^2\psi_2} \quad .$$

Then denoting

$$k_2 = \sqrt{\frac{x_2-1}{x_2-x_3}} \quad ,$$

we find

$$J_o = \frac{-2}{\sqrt{(K^2-\Omega^2)(x_2-x_3)}} \int_{\psi_2}^{\pi/2} \frac{d\psi}{\sqrt{1-k_2^2\sin^2\psi}} \quad ,$$

or

$$J_o = -\frac{2}{\sqrt{(K^2-\Omega^2)(x_2-x_3)}} \left[F(k_2) - F(\psi_2, k_2)\right] \quad , \qquad \text{(B-9)}$$

where F (k) is the complete elliptic integral of the first kind. Similarly

$$J_1 = \frac{-2}{\sqrt{(K^2-\Omega^2)(x_2-x_3)}} \int_{\psi_2}^{\pi/2} \frac{x_3 + (x_2-x_3)[1-k_2^2\sin^2\psi]}{\sqrt{1-k_2^2\sin^2\psi}}\, d\psi \quad ,$$

or

(B-10)

$$J_1 = -\frac{2}{\sqrt{(K^2-\Omega^2)(x_2-x_3)}} \left\{x_3\left[F(k_2) - F(\psi_2, k_2)\right] + (x_2-x_3)\left[E(k_2) - E(\psi_2, k_2)\right]\right\} \quad ,$$

where E(k) is the complete elliptic integral of second kind. Finally

$$J_{-1} = -\frac{2}{\sqrt{(K^2-\Omega^2)(x_2-x_3)}} \int_{\psi_2}^{\pi/2} \frac{d\psi}{x_2\left[1-\frac{x_2-1}{x_2}\sin^2\psi\right]\sqrt{1-k_2^2\sin^2\psi}} \quad ,$$

or

$$J_{-1} = \frac{2}{x_2\sqrt{(K^2-\Omega^2)(x_2-x_3)}}\left[\Pi(\alpha_2^2, k_2) - \Pi(\psi_2, \alpha_2^2, k_2)\right] , \qquad \text{(B-11)}$$

where $\Pi(\alpha^2, k)$ is the complete elliptic integral of third kind, and

$$\alpha_2^2 = \frac{x_2-1}{x_2} . \qquad \text{(B-12)}$$

The incomplete elliptic integrals of first, second, and third kind are tabulated functions (see References 7 and 9 for example). The complete elliptic integral of third kind can also be evaluated in terms of Heuman's Lambda Function, a tabulated function.

Consider Case A: $K > \Omega$, $x_3 < x_2 < x < 1$. Then we have

$$k_1^2 > 0 \quad \text{and} \quad k_1^2 < \alpha_1^2 < 1 .$$

Case B: $K > \Omega$, $x_3 < 1 < x < x_2$. Then

$$k_2^2 > 0 \quad \text{and} \quad k_2^2 < \alpha_2^2 < 1 .$$

For both Case A and B, from Reference 4, No. 413.01, we have

$$\Pi(\alpha^2, k) = \frac{\pi\alpha\Lambda_o(\xi, k)}{2\sqrt{(\alpha^2-k^2)(1-\alpha^2)}} . \qquad \text{(B-13)}$$

Here Λ_o is Heuman's Lambda Function, and $\sin\xi = \sqrt{\frac{\alpha^2-k^2}{\alpha^2(1-k^2)}}$.

Case C: $K < \Omega$, $x_2 < x < 1 < x_3$. Then $\alpha_2^2 < 0$.

Case D: $K < \Omega$, $1 < x < x_2 < x_3$. Then $\alpha_1^2 < 0$.

For both Case C and D, from Reference 4, No. 410.01, we have

$$\Pi(\alpha^2, k) = \frac{k^2 F(k)}{k^2-\alpha^2} - \frac{\pi\alpha^2\Lambda_o(\eta, k)}{2\sqrt{\alpha^2(1-\alpha^2)(\alpha^2-k^2)}} , \qquad \text{(B-14)}$$

with $\sin\eta = \sqrt{\frac{\alpha^2}{\alpha^2-k^2}}$.

APPENDIX C

CONDITION FOR MERIDIAN CURVE OF CUSP

Denote by x_0 the value of x for zero slope, and recall that x_2 is the value of x for infinite slope. Then the cusp condition is $x_0 = x_2$. From equation (14) (with $\rho_f = 0$)

$$x_0 = 1 - \frac{2}{K}\sqrt{1 - C^2}$$

while x_2 is given by equation (17). Hence the condition $x_0 = x_2$ is given by

$$\left[\frac{\Omega^2 - K^2}{2}\left(1 - \frac{2}{K}\sqrt{1-C^2}\right) - H\right]^2 = H^2 - C^2(\Omega^2 - K^2) .$$

Squaring, collecting terms, and dividing out $(\Omega^2 - K^2)$, we are left with the expression

$$K^2(1 - \Omega) + \Omega^2(1-C^2) - (K^2 + \Omega^2 - 4\Omega)\frac{K}{2}\sqrt{1-C^2} = 0 ,$$

which is a quadratic in either Ω or $1-C^2$. As a quadratic in Ω, we have

$$\Omega^2\left(\frac{K}{2}\sqrt{1-C^2}\, x_0\right) + \Omega K^2 x_0 - \frac{K^4}{4}\left(\frac{4}{K^2} - 1 + x_0\right) = 0 .$$

By the quadratic formula

$$\Omega = -\frac{K}{\sqrt{1-C^2}}\left\{1 \pm \sqrt{1 + \frac{2}{K}\frac{1-C^2}{\left(\frac{1 - \frac{K}{2}\sqrt{1-C^2}}{1 - \frac{2}{K}\sqrt{1-C^2}}\right)}}\right\} .$$

To have $\Omega > 0$ we take the lower sign. Rewriting the radicand we obtain finally

$$\Omega = \frac{K}{\sqrt{1-C^2}}\left\{\sqrt{\frac{C^2}{1 - \frac{2}{K}\sqrt{1-C^2}}} - 1\right\} .$$

In terms of x_0

$$\Omega = \frac{2}{1 - x_0}\left\{\sqrt{\frac{C^2}{x_0}} - 1\right\}, \quad K = \frac{2\sqrt{1-C^2}}{1-x_0} .$$

REFERENCES

1. Green, A. E. and T. E. Adkins: Large Elastic Deformations and Non-Linear Continuum Mechanics. Oxford University Press, 1960.

2. Hearmon, R. F. S. : The Elastic Constants of Anisotropic Materials. Reviews of Modern Physics, Vol. 18, No. 3, July 1946. p. 409-440.

3. Schuerch, H. U., O. R. Burggraf, and A. C. Kyser (Astro Research Corporation): A Theory and Applications of Filamentary Structures. NASA TN D-1692 (N63-11057), December 1962. Available from Office of Technical Services, $2.25.

4. Williams, M. L., G. Gerard, and G. A. Hoffman: III. The Effect of Filamentary Materials on Pressure Vessel Design. Proceedings of XIth International Astronautical Congress (Stockholm, Sweden, August 15-20, 1960), Vol. I, Springer-Verlag, Berlin, 1961. p. 146.

5. Schuerch, H. U. (Astro Research Corporation): Space Structure Design with Composite Materials. ARS Preprint 1096-60, April 1960.

6. Zickel, J.: Isotensoid Pressure Vessels. ARS Journal, Vol. 32, No. 6, June 1962, p. 950-951.

7. Byrd, P. F., and M. D. Friedman: Handbook of Elliptic Integrals for Engineers and Physicists. Springer-Verlag, Berlin, 1954.

8. Kyser, A. C. (Astro Research Corporation): A Contribution to the Theory of Pressure Stabilized Structures. NASA TN D-1919, April 1963.

9. Selfridge, R. G., and J. E. Mayfield: Table of the Incomplete Elliptic Integral of the Third Kind. Dover Publications, Inc., New York, 1958.

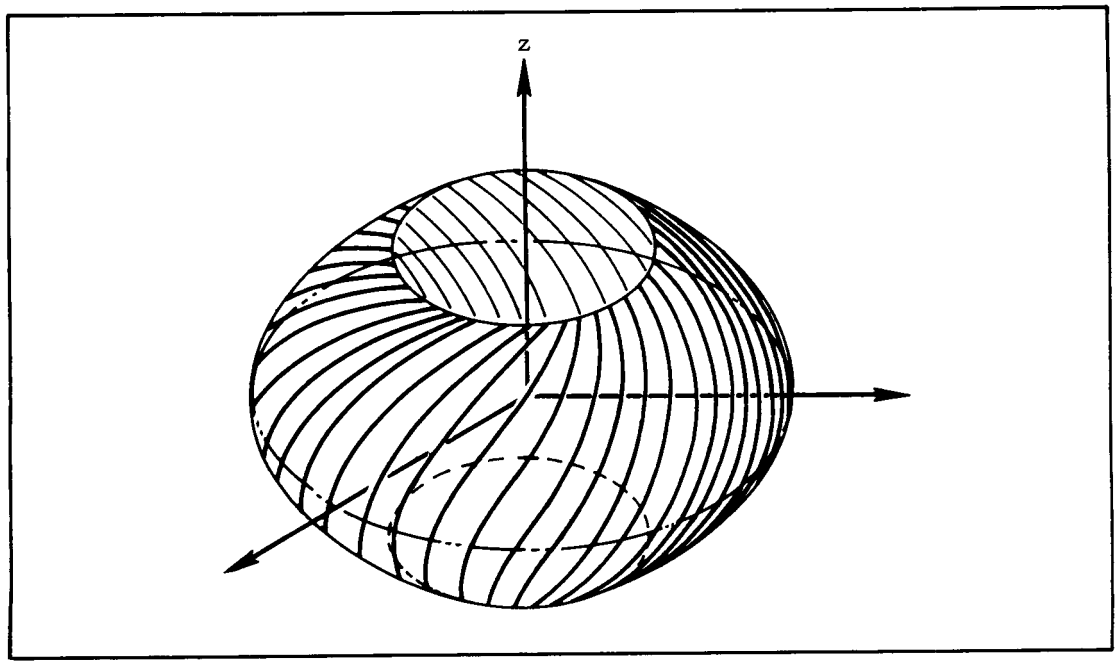

Figure 1. Monotropic Membrane of Revolution.

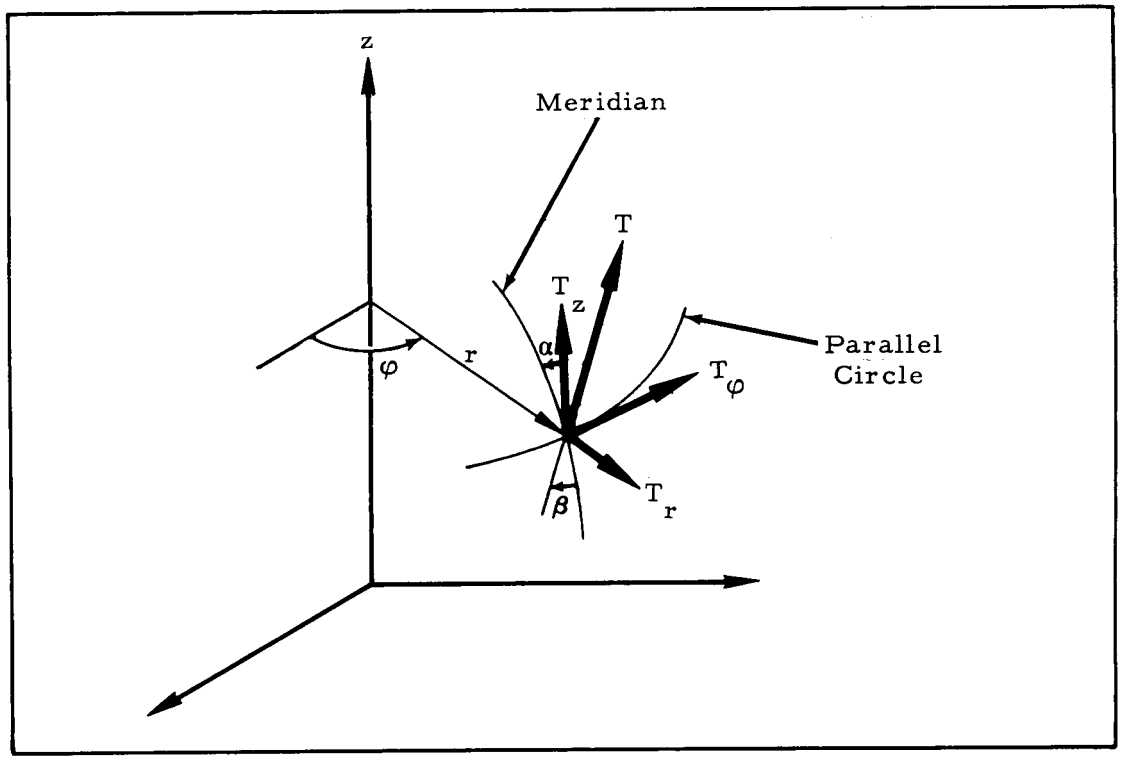

Figure 2. Coordinates and Notations.

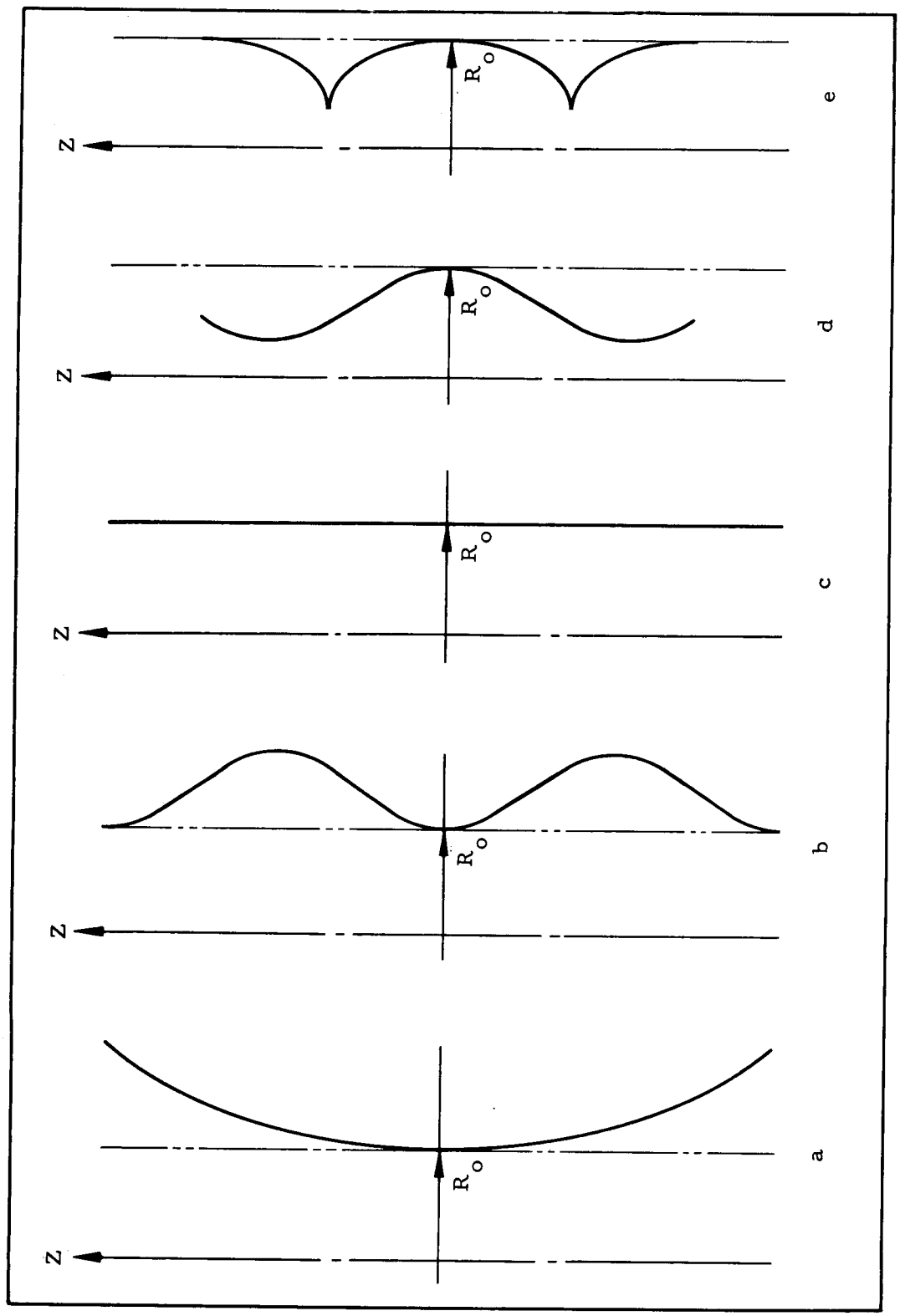

Figure 3. Undulated Meridional Shapes.

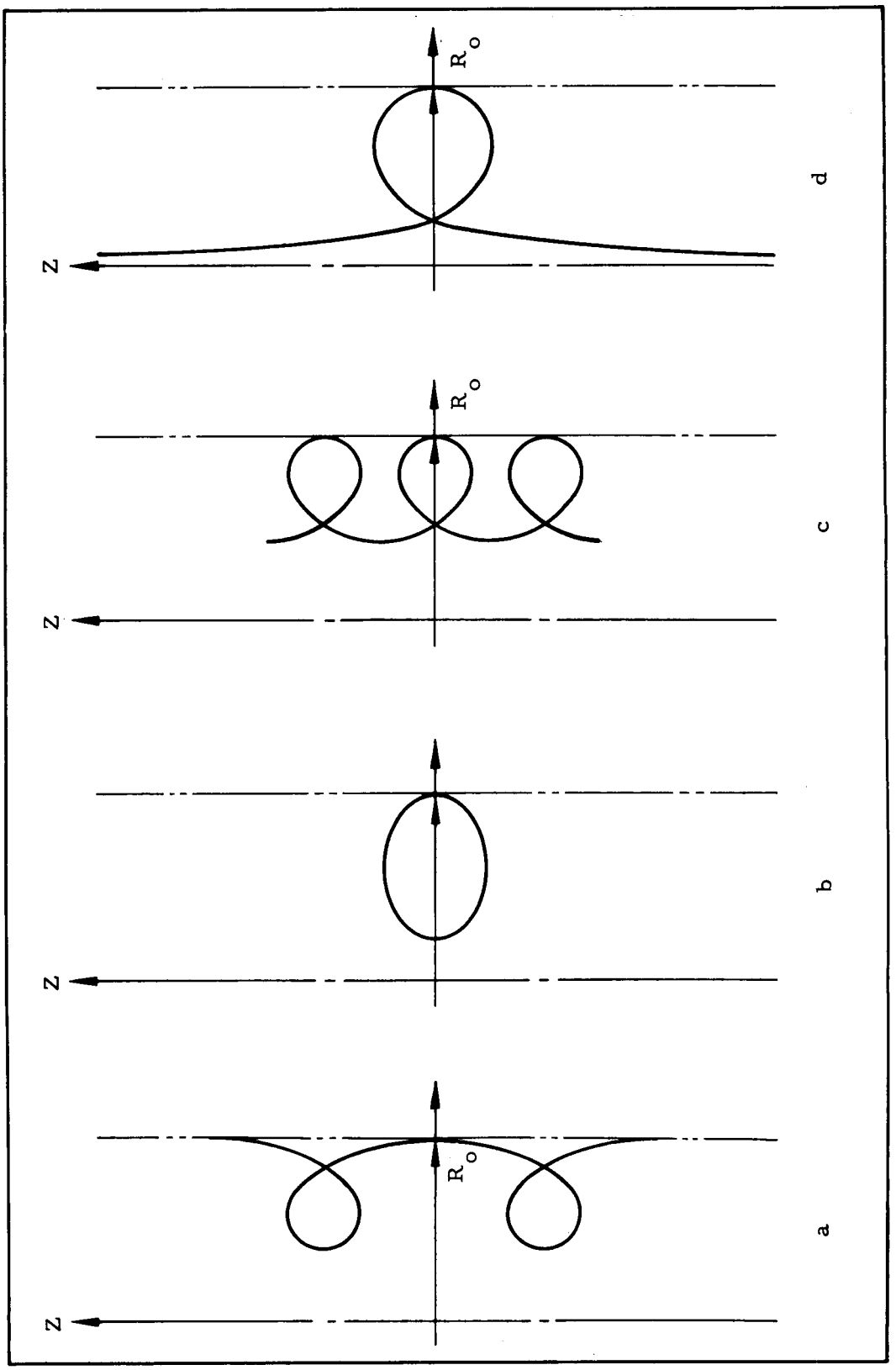

Figure 4. Looped Meridional Shapes.

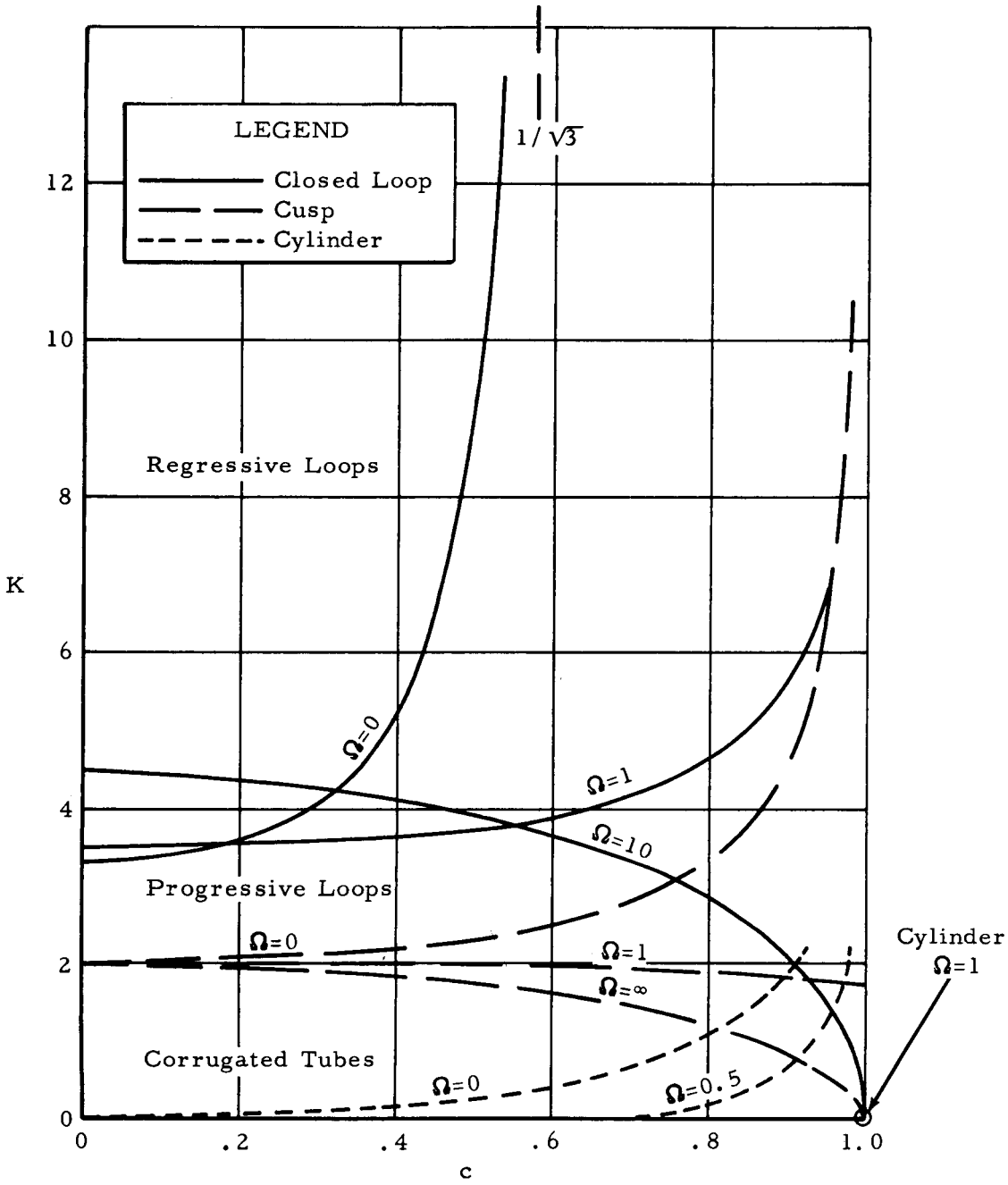

Figure 5. Domains for Various Classes of Meridian Curves.

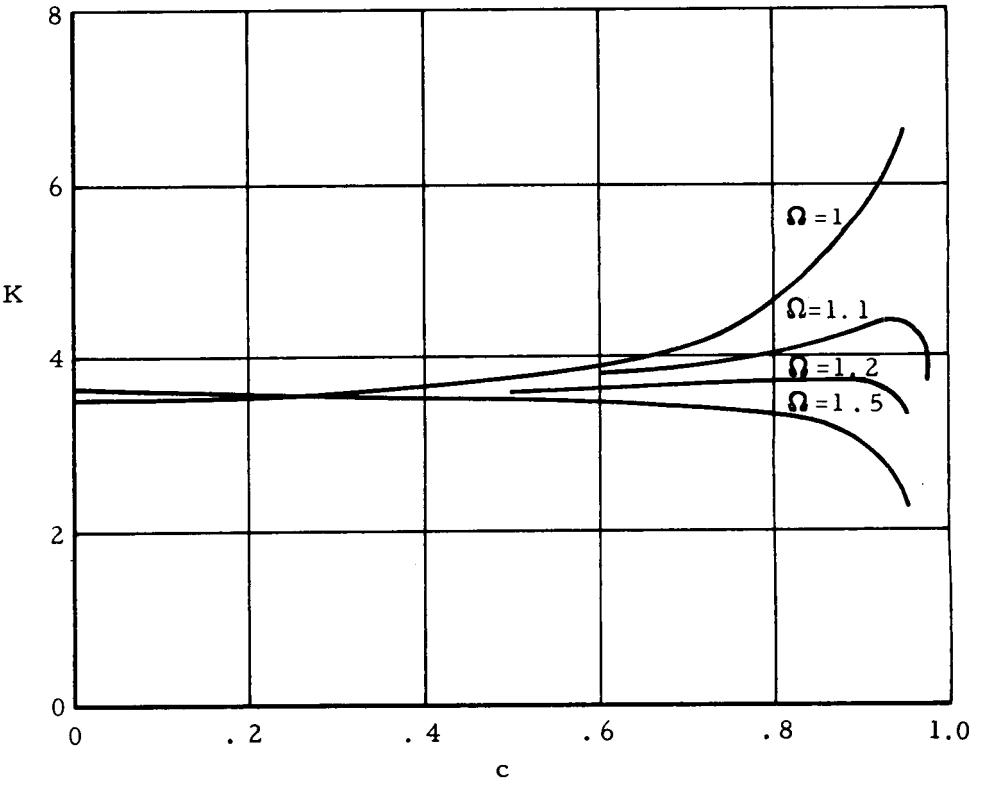

Figure 6. Closed Loop Conditions for $\Omega \lesssim 1$.

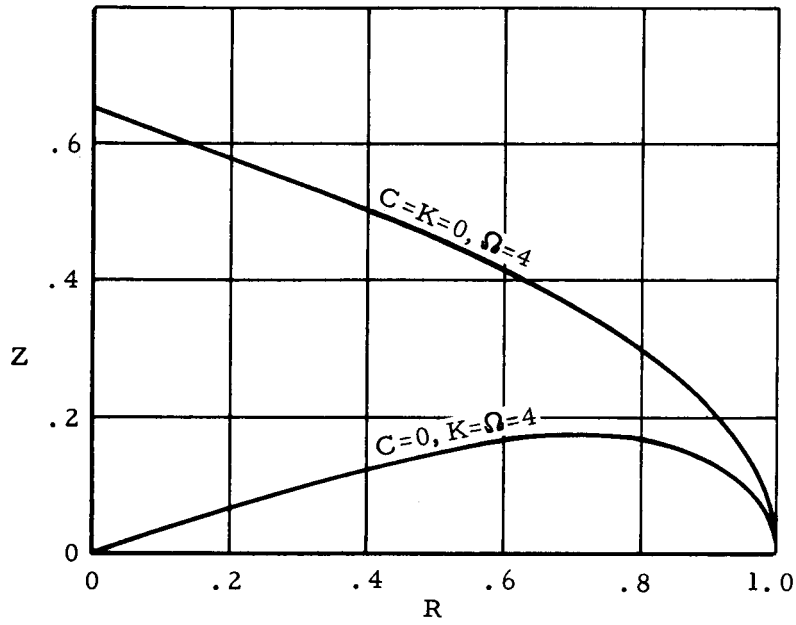

Figure 7. Sample Meridian Curves, C = 0.

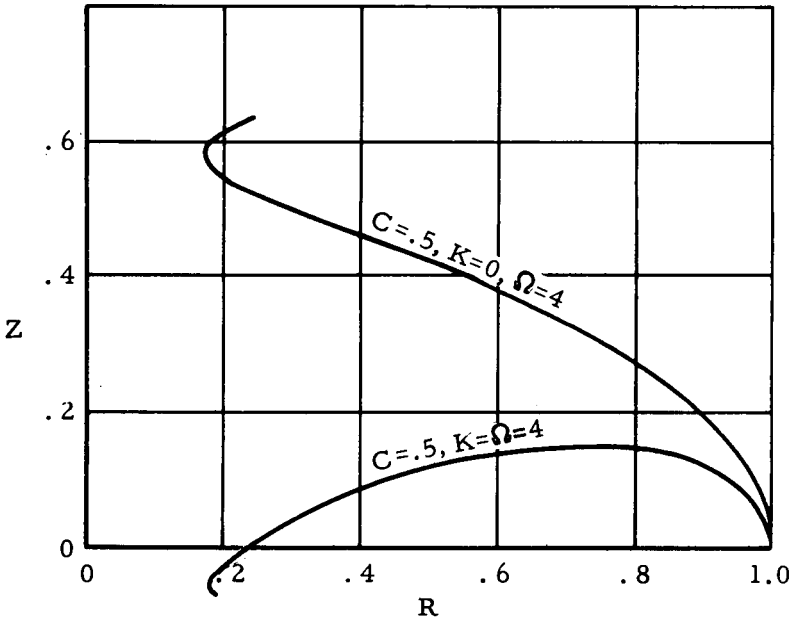

Figure 8. Sample Meridian Curves, C = 0.5.

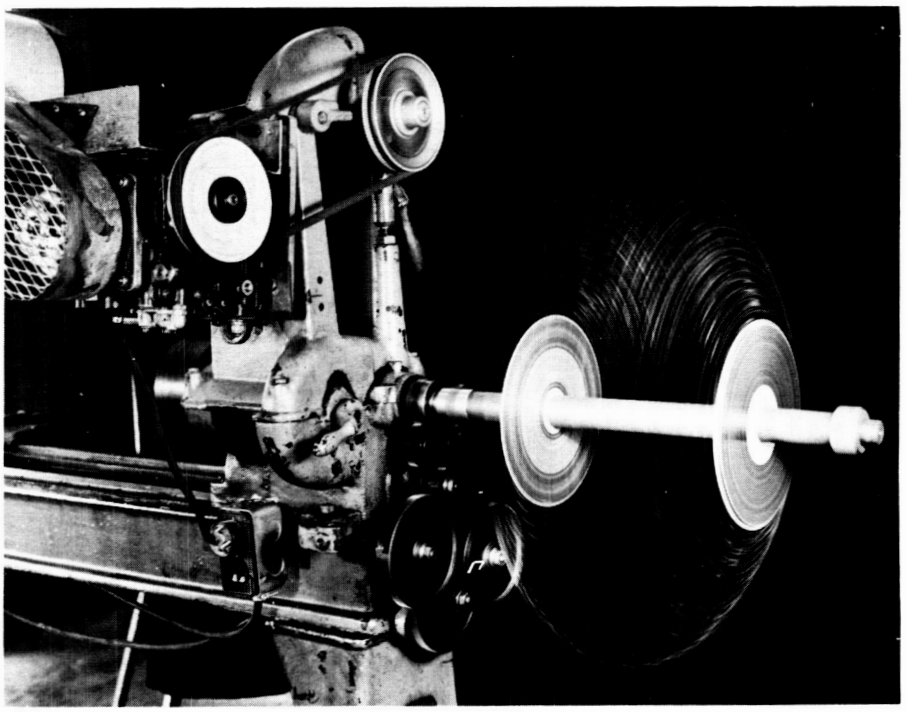

Figure 9. Test Setup, Rotating Chain, Time Exposure.

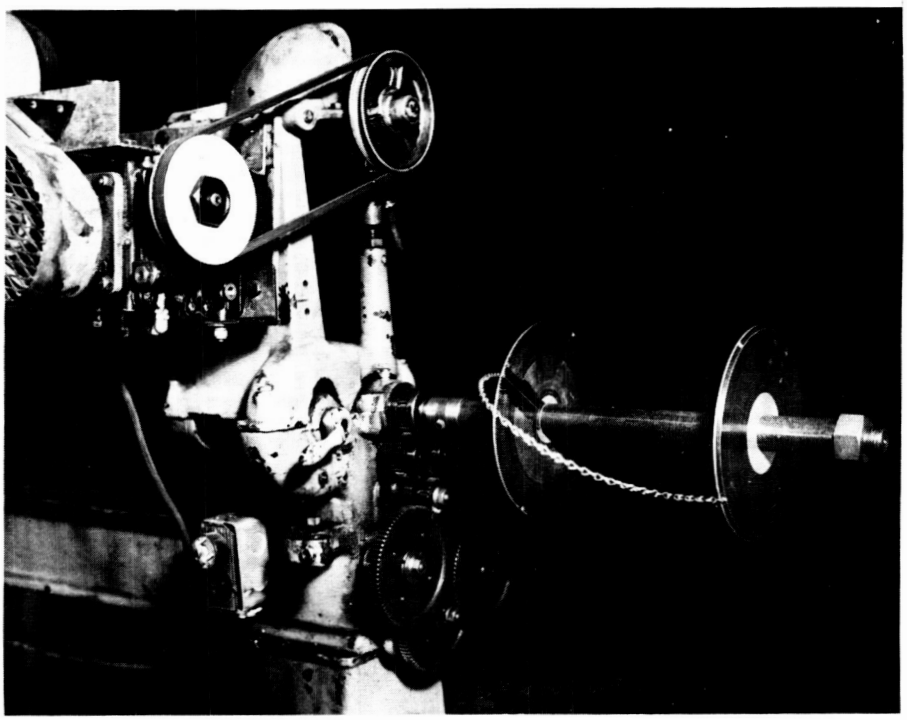

Figure 10. Rotating Chain, Flash Exposure.

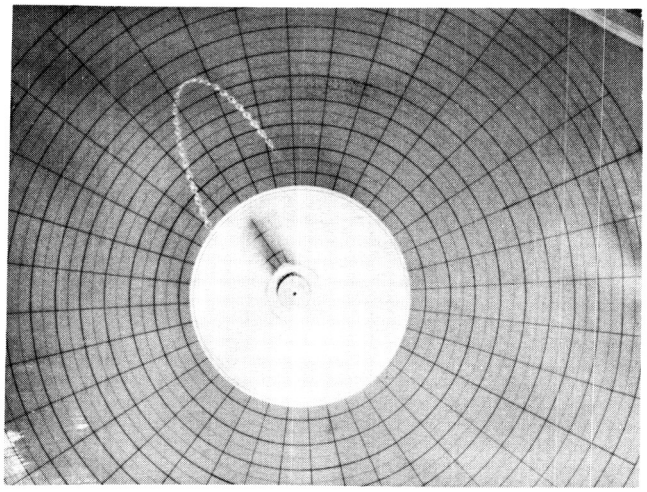

a

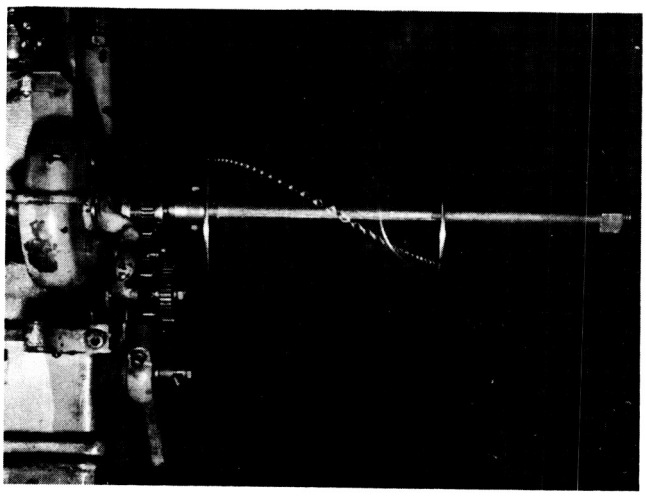

b

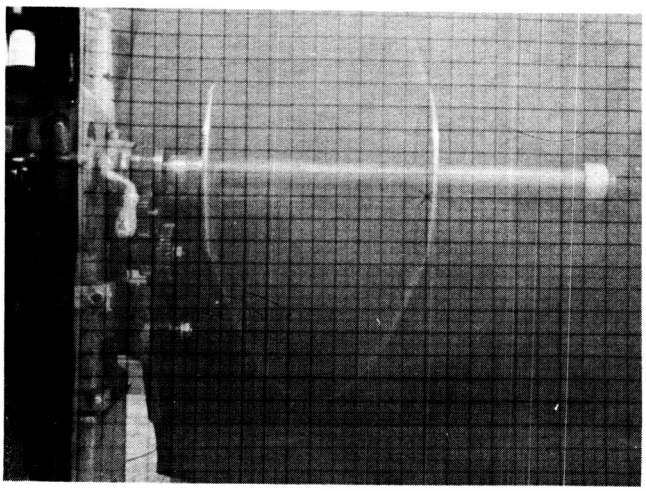

c

Figure 11. Experiment- Rotating Chain, $C = .5$, $\Omega = 4$, $K = 0$.

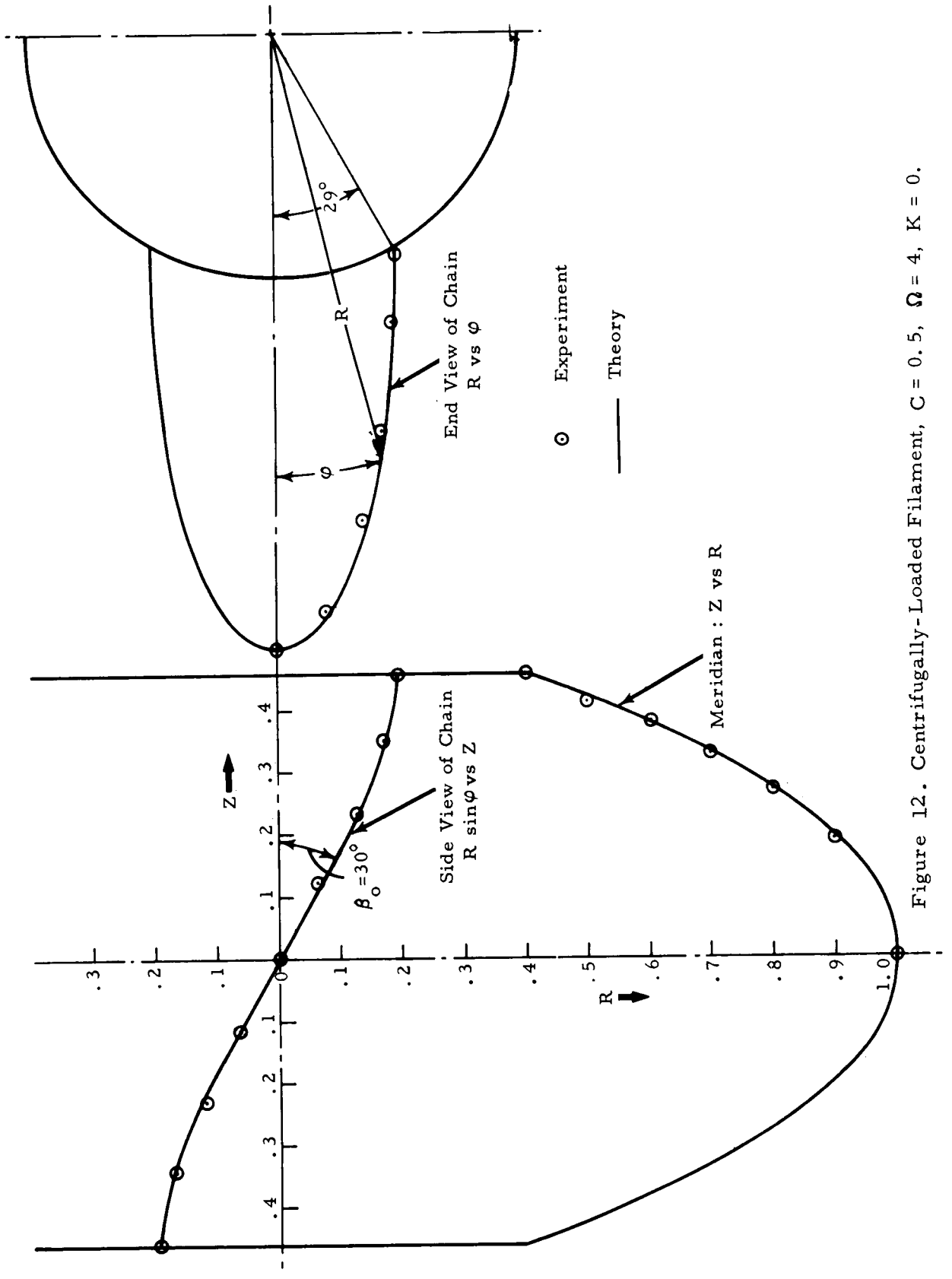

Figure 12. Centrifugally-Loaded Filament, C = 0.5, Ω = 4, K = 0.

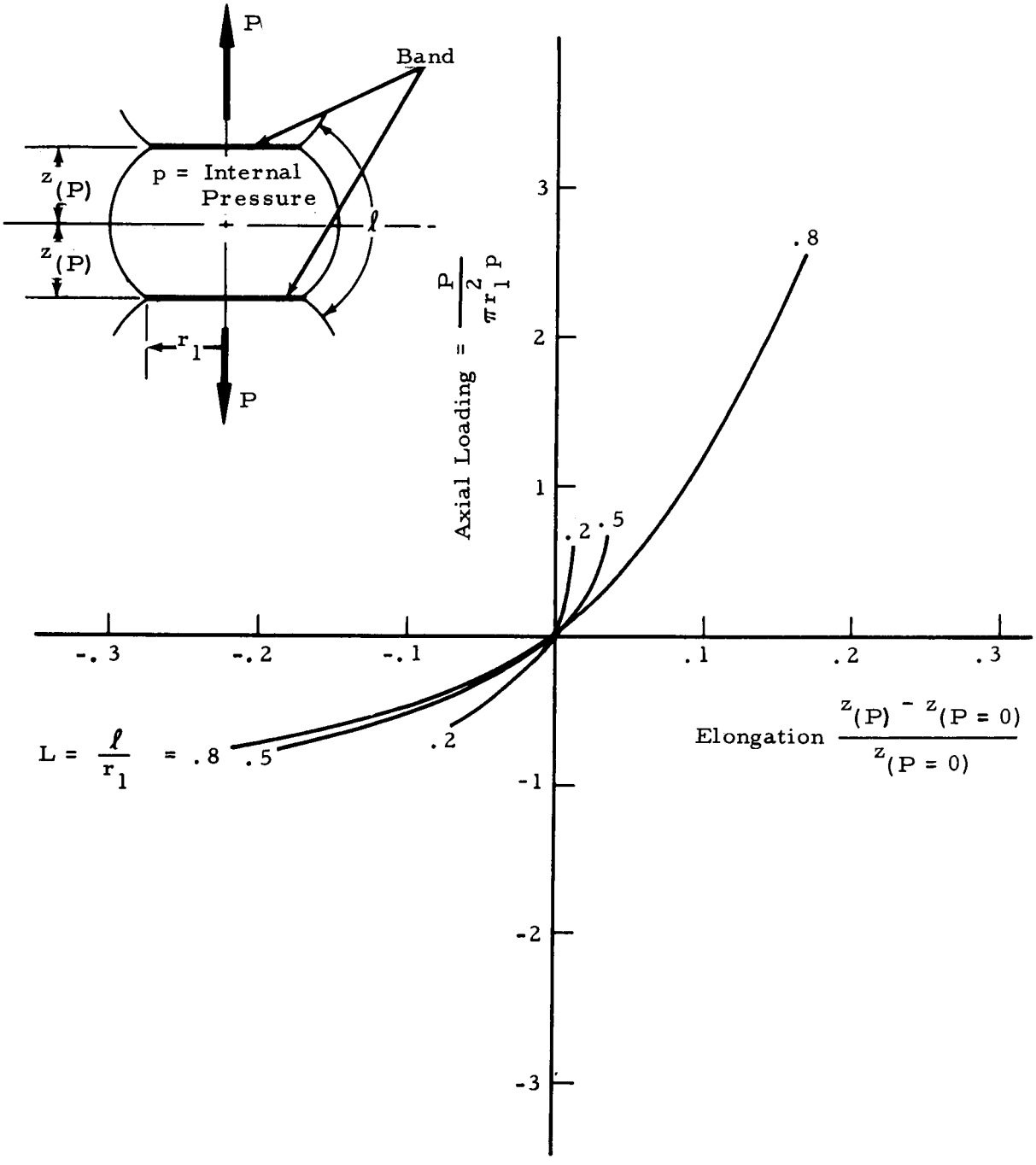

Figure 13. Load-Deformation Characteristics of Pressure Stabilized, Corrugated Cylinder.

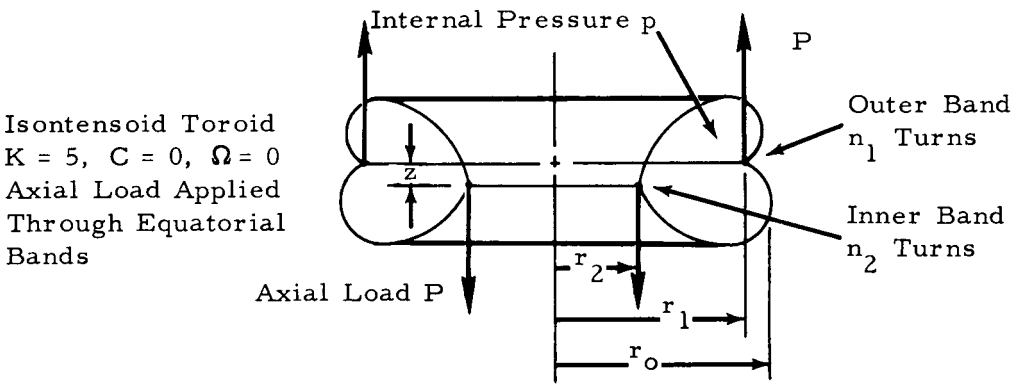

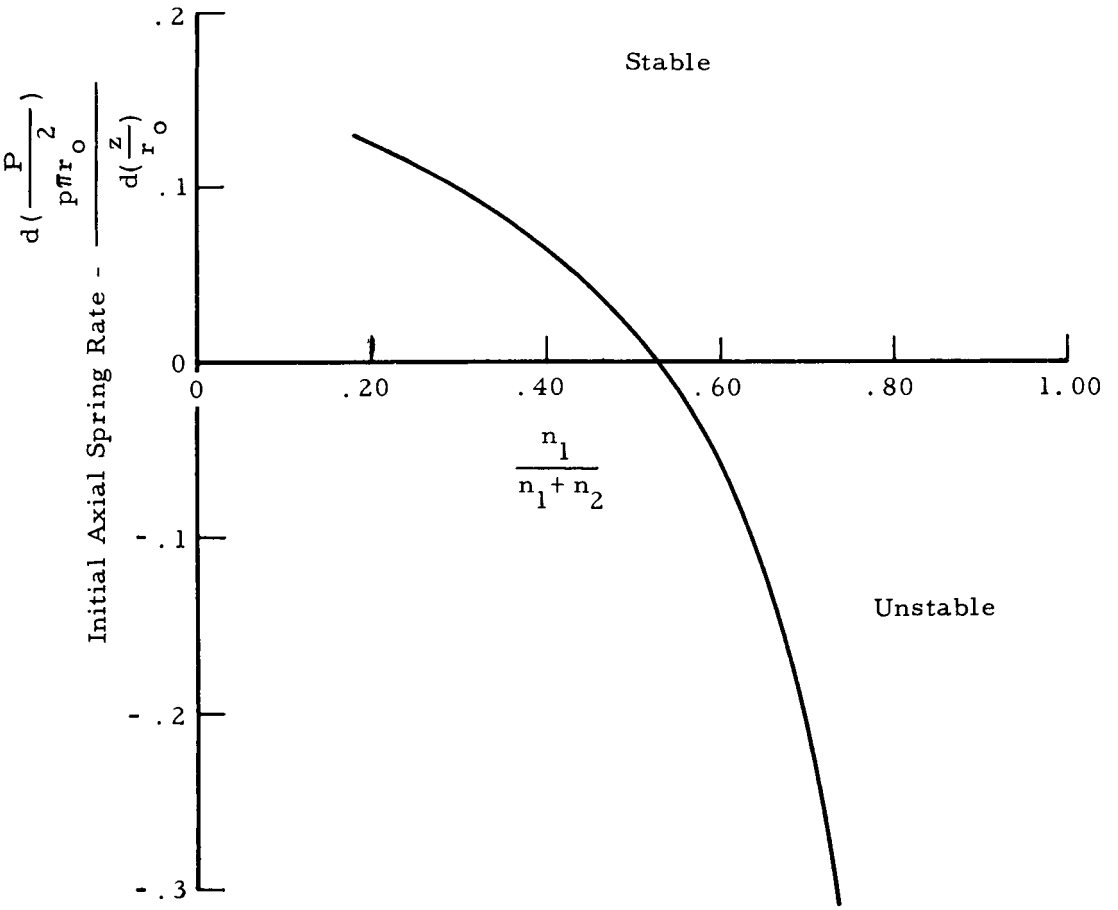

Figure 14. Initial Spring-Rate of Axially-Loaded Isotensoid Toroids in Function of Design Parameter $\frac{n_1}{n_1 + n_2}$.